Characterization of Submicron Particles of Tetragonal $BaTiO_3$

Reza Asiaie,[†] Weidong Zhu,[‡] Sheikh A. Akbar,[‡] and Prabir K. Dutta*,[†]

Departments of Chemistry and Materials Science and Engineering, The Ohio State University, 120 W. 18th Avenue, Columbus, Ohio 43210

Received July 18, 1995. Revised Manuscript Received October 10, 1995[⊗]

Barium titanate ($BaTiO_3$) powders of varying particle sizes were grown under hydrothermal conditions at a temperature of 240 °C. This was accomplished by varying the hydroxide concentration of the reaction medium as well as the time required for synthesis. The spectroscopic, thermal, and microscopic characteristics of three $BaTiO_3$ powders with average particle sizes 0.09, 0.3, and 0.5 μm were examined. Transmission electron microscopy indicated that all the particles were of single domain. The powder with smallest particle sizes (0.09 μm) contained unreacted titanium dioxide, whereas the larger particles (0.3, 0.5 μm) were pure barium titanate. The Raman spectra showed that all these crystals were tetragonally distorted. Infrared spectra showed primarily Frohlich modes, whose intensities also decreased with particle size. Analysis of the broadening of the powder diffraction patterns suggested that the $BaTiO_3$ powders exhibited small strains. Differential scanning calorimetry showed a decrease in enthalpy of transition (ΔH) values with particle size. The particle size dependence on ΔH is attributed to the transition from a polar to a nonpolar state which occurs due to the bulk dipoles disordering due to interaction with the surface dipoles.

Introduction

Ferroelectric $BaTiO_3$ is extensively used in microelectronics and integrated optics technologies.[1] The conventional synthesis of barium titanate compounds involve high temperature (∼1200 °C) calcination of solid mixtures of barium carbonate and titanium dioxide.[2] Fabrication of advanced and complex electronic components requires homogeneous and pure powders with uniform and fine particle sizes.[3] Various synthesis methods to accomplish this has been reported.[4−8] Controlled stoichiometry precursor materials such as mixed Ba−Ti oxalates,[5] citrates,[6] and alkoxide salts[7,8] can be heat treated to prepare $BaTiO_3$ powders. Because of the enhanced atomic level contact between Ba and Ti by the participating ligands, lower temperatures are required to form $BaTiO_3$.[9] Direct hydrothermal synthesis of $BaTiO_3$ from mixtures of $Ba(OH)_2$, TiO_2, or gels of Ba−Ti acetate in a basic aqueous solution can be accomplished at reaction temperatures of 80−150 °C.[10] The lower processing temperature has its advantages in producing finer particles and allowing more uniformity in grain microstructure as well as help form thin films on various substrates.[11]

As the formation of $BaTiO_3$ powders by different methods has evolved over the past two decades, its exact structural form has also been debated. The crystallographic forms of $BaTiO_3$ are well known. Below 130 °C, it undergoes transformation from a cubic into a tetragonal structure, which remains so until 0 °C, at which point it transforms to an orthorhombic form.[12] Thus, at room temperature, $BaTiO_3$ should exist in its tetragonal form. The difference between the cubic and tetragonal form is readily ascertained from the powder X-ray diffraction pattern, since the tetragonal form shows distinctive splitting of certain peaks.[13] As the particle size becomes smaller, broadening effects can make this splitting difficult to determine.[14] The literature indicates that low-temperature synthesis methods result in a cubiclike structure. This metastable form

[†] Department of Chemistry.
[‡] Department of Materials Science and Engineering.
[⊗] Abstract published in *Advance ACS Abstracts,* November 15, 1995.

(1) (a) Parker, L. H.; Tasch, A. F. *IEEE Circuit Device Mag.* **1990**, 17. (b) Dey, S. K.; Lee, J. J. *IEEE Trans. Electron Devices* **1992**, *ED-39*, 1607. (c) Wu, S. Y.; Takei, W. J.; Francombe, M. H. *Ferroelectrics* **1976**, *10*, 209.
(2) Bauger, A.; Mutin, J. C.; Niepce, J. C. *J. Mater. Sci.* **1983**, *18*, 3041.
(3) Phule, P. P.; Risbud, S. H. *J. Mater. Sci.* **1990**, *25*, 1169.
(4) Hennings, D. *Electroceram., Brit. Ceram. Proc.* **1989**, *41*, 1.
(5) (a)Claubaugh, W. S.; Swiggard, E. M.; Gilchrist, R. *J. Res. Natl. Bur. Std.* **1956**, *56*, 289. (b) Stockenhuber, M.; Mayer, H.; Lercher, J. A. *J. Am. Ceram. Soc.* **1993**, *76*, 1185.
(6) (a) Mulder, B. J. *Ceram. Bull.* **1970**, *49*, 990. (b) Hennings, D.; Mayr, W. *J. Solid State Chem.* **1978**, *26*, 329.
(7) Mazdiyasni, K. S.; Brown, L. M. *J. Am. Ceram. Soc.* **1972**, *55*, 633.
(8) Kirby, K. W. *Mater. Res. Bull.* **1988**, *23*, 881.
(9) (a) Kumar, S.; Messing, G. L.; White, W. B. *J. Am. Ceram. Soc.* **1993**, *76*, 617. (b) Dutta, P. K.; Twu, J.; Gallagher, P. *Chem. Mater.* **1993**, *5*, 1739. (c) Zhong, Z.; Gallagher, P. K. *J. Mater. Res.* **1995**, *10*, 945.
(10) (a) Flaschen, S. S. *J. Am. Chem. Soc.* **1955**, *77*, 6194. (b) Christensen, A. N. *Acta. Chem. Scand.* **1970**, *24*, 2447. (c) Kutty, T. R. N.; Balachandran, R. *Mater. Res. Bull.* **1984**, *19*, 1479. (d) Hennings, D.; Rosenstein, G.; Schreinemacher, H. *J. Eur. Ceram. Soc.* **1991**, *8*, 107. (e) Kajiyoshi, K.; Ishizawa, N.; Yoshimura, M. *J. Am. Ceram. Soc.* **1991**, *74*, 369. (f) Dutta, P. K.; Gregg, J. R. *Chem. Mater.* **1992**, *4*, 843. (g) Chaput, F.; Boilot, J. P.; Beauger, A. *J. Am. Ceram. Soc.* **1990**, *73*, 942. (h) Shvets, L. I.; Ovramenko, N. A.; Ovcharenko, F. D. *Dokl. Akad. Nauk. SSSR* **1979**, *248*, 889.
(11) (a) Bacsa, R. R.; Dougherty, J. P.; Pilione, L. *J. Appl. Phys. Lett.* **1993**, *63*, 1053. (b) Bendale, P.; Venigalla, S.; Ambrose, J. R.; Verink, Jr. E. D.; Adair, J. H. *J. Am. Ceram. Soc.* **1993**, *76*, 2619.
(12) Moulson, A. J.; Herbert, J. M. *Electroceramics*, Chapman and Hall: London, 1992; p 69.
(13) Murugaraj, P.; Kutty, T. R. N. *Mater. Res. Bull.* **1985**, *20*, 1473.
(14) Klug, H. P.; Alexander, L. E. *X-Ray Diffraction Procedure for Polycrystalline and Amorphous Materials*; Carnegie-Mellon University Press: New York, 1973; p 618.

0897-4756/96/2808-0226$12.00/0

can be converted to the thermodynamically stable tetragonal form by annealing at higher temperatures (1100 °C) and then cooling through the Curie transition.[15] It has been shown that the hydrothermal synthesis performed at 200 °C or higher promotes the formation of tetragonal phase.[10e,h] For temperatures as high as 600 °C, tetragonal $BaTiO_3$ can be synthesized with submillimeter sizes.[10b]

Considerable effort has been spent in understanding the factors responsible for stabilization of the metastable cubic form of $BaTiO_3$ at ambient conditions. Three factors discussed in the literature are the size of the crystallite, defects in the crystallite, and the presence of a surface layer.[15−17] We have reported earlier that $BaTiO_3$ synthesized hydrothermally at 240 °C possesses a tetragonal structure.[10f] In this paper, we examine the properties of $BaTiO_3$ of various particle sizes synthesized by this methodology, with the goal of analyzing the tetragonal to cubic transition as a function of size. By modifying the basicity of the initial solution, particles with average sizes in the range 0.09−0.5 μm were produced. On the basis of the structural, thermal, strain, and defect characteristics as well as microstructure of these particles, we find in agreement with the recent literature[18] that the TiO_6 octahedra remain distorted at all particle sizes, though there is a transformation from a polar to a nonpolar structure below a critical particle size.

Experimental Section

Materials. Reagents (99.999% pure) of $BaCl_2$ and titanium(IV) isopropoxide were obtained from Alfa/Johnson Matthey, Inc. NaOH was acquired from J. T. Baker Inc.

Synthesis. Barium titanate powders were synthesized in 23 mL digestion bombs (Parr Instrument Co.) at 240 °C. The following synthesis procedure and reagent compositions were used: 0.005 mol of $BaCl_2$, 0.003 mol of hydrated titanium oxide, and varying amounts of NaOH in 10 mL of degassed deionized water. Hydrated titanium oxide was prepared by hydrolyzing titanium(IV) isopropoxide with 1 M hydrochloric acid followed by washing the precipitate by centrifugation with deionized water. The mixture was purged with N_2 gas for about 5 min before the addition of NaOH. After the addition of the base, the bomb was immediately sealed and placed in an oven at 240 °C.

Starting with 0.003 and 0.005 mol of NaOH, $BaTiO_3$ powders of 0.09 and 0.3 μm average particle sizes, respectively were obtained after 1 week of heating. The 0.5 μm size particles were prepared by modifying the synthesis procedure used to obtain the 0.3 μm size particles. This was done by adding 0.003 mol of NaOH to the product mixture after 1 week of synthesis and continued heating for another week. After the appropriate heating period, the samples were washed with water to remove Cl^-, which was confirmed by chemical analysis and X-ray fluorescence. The Ba and Ti contents were determined by ICP according to the procedure described by Farinas and Barba,[19] using a Perkin Elmer Optima 3000XL spectrometer. The $BaTiO_3$ powders were dissolved in HCl and heated at 160 °C for 14 h. $BaCl_2$ (Alfa/Johnson Matthey, Inc.) and Ti metal (Aldrich Chemical Co., Inc.) were used to prepare the standard solutions.

Characterization. Diffraction patterns were acquired from a Rigaku Geigerflex D/Max-3B powder diffractometer with nickel filtered Cu Kα (1.5405 Å) source. The calorimetric measurements were performed with a DSC 910S differential scanning calorimeter (TA Instruments). A SSC5200 thermal analysis system with Seiko TG/DTA 320 module was used for the thermogravimetric experiments.

The microstructure and morphology of the powders and the sintered samples were investigated using Hitachi S-4000 scanning electron microscope equipped with a field emission gun. An accelerating voltage of 5 kV was used. A gold layer was sputter coated on the samples for the SEM analysis. The particle sizes were the average values of the diameters of at least 20 particles (taken along the diagonals of the micrograph) from SEM micrographs using linear intercept method.

Lattice images and convergent beam diffraction patterns of the particles were obtained using a Hitachi high-resolution electron microscope (H-9000 NAR) with 1.8 Å resolution. The microscope was operated at a voltage of 300 kV. A small amount of the powder was first suspended with isopropanol in a 3.5 mL vial and allowed to settle for 24 h. Then a drop of the supernatant solution was placed onto the holey carbon grid.

The infrared spectra were obtained on a Mattson Cygnus FT-IR equipped with a MCT detector in a controlled-atmosphere cell. Raman spectra were obtained using a Spectra-Physics Model 171 Ar ion laser as the excitation source. For all samples, the 514.5 nm line at power of 80 mW was used. A Spex 1403 double monochromator and a RCA C131034 GaAs photon-counting photomultiplier tube was used to filter and detect the scattered light. The temperature-controlled Raman experiments were performed with a Raman cell fabricated from Macor that had a copper insert as a heating element and was sealed with a quartz window.

Lattice parameter and lattice strain calculations were done from the diffraction patterns obtained on a Scintag powder X-ray diffractometer (PAD-V). Si powder (99.999%, Johnson Matthey) was used as the internal calibration standard to correct for line position. LaB_6 (99.95%, Johnson Matthey) was used as the external standard to correct for instrumental broadening. Prior to use, the LaB_6 was annealed to 800 °C in Ar to eliminate any residual strains. Lattice refinement method (DMS-2000 software) was used to compute the lattice parameters. The lattice strains were calculated using Hall−Williamson or Gaussian squared method assuming a Gaussian−Gaussian profile. The peaks were first deconvoluted, and the full widths at half-maximum (fwhm) of the peaks were calculated by profile fitting. Assuming a Gaussian peak profile, the Hall−Williamson method uses a square relationship written as[20]

$$(\beta_{1/2} \cos \theta/\lambda)^2 = (0.89/d)^2 + 16\epsilon^2(\sin \theta/\lambda)^2$$

where $\beta_{1/2}$ is the true breadth of diffraction line at half-maximum intensity using Warran's method for instrumental correction,[20] d the particle size, and ϵ the elastic strain. When $(\beta_{1/2} \cos \theta/\lambda)^2$ is plotted vs $(4 \sin \theta/\lambda)^2$ for different diffraction planes, a linear fit is expected. From the slope of this line, lattice strains were obtained.

Results

Hydrothermal Synthesis of $BaTiO_3$ Powders. In a previous study, we have reported on the formation of tetragonal $BaTiO_3$ at 240 °C under hydrothermal conditions.[10f] The role of various inorganic barium salts (chloride, bromide, iodide, nitrate, and acetate), barium hydroxide, Ba/Ti ratio, and titanium source was subse-

(15) (a) Bacsa, R.; Ravindranathan, P.; Dougherty, J. P. *J. Mater. Res.* **1992**, *7*, 423. (b) Vivekanandan, R.; Philip, S.; Kutty, T. R. N. *Mater. Res. Bull.* **1986**, *22*, 99. (c) Vivekanandan, R.; Kutty, T. R. N. *Powder Technol.* **1989**, *57*, 181. (d) Naka, S.; Nakakita, F.; Suwa, Y.; Inagaki, M. *Bull. Chem. Soc. Jpn.* **1973**, *47*, 1168.

(16) (a) Begg, B. D.; Vance, E. R.; Cassidy, D. J.; Nowotny, J.; Blairs, S. *Ceram. Trans.* **1994**, *41*, 169. (b)Yamamoto, T.; Urabe, K.; Banno, H. *Jpn. J. Appl. Phys.* **1993**, *32*, 4272.

(17) (a) Goswami, A. K. *J. Appl. Phys.* **1969**, *40*, 619. (b) Callaby, D. R. *J. Appl. Phys.* **1966**, *37*, 2295.

(18) Schlag, S.; Eicke, H. F. *Solid State Commun.* **1994**, *91*, 883.

(19) Farinas, J. C.; Barba, M. F. *Mikrochim. Acta* **1989**, *3*, 299.

(20) Cullity, B. D. *Elements of X-ray Diffraction*, 2nd ed., Addison-Wesley: London, 1978.

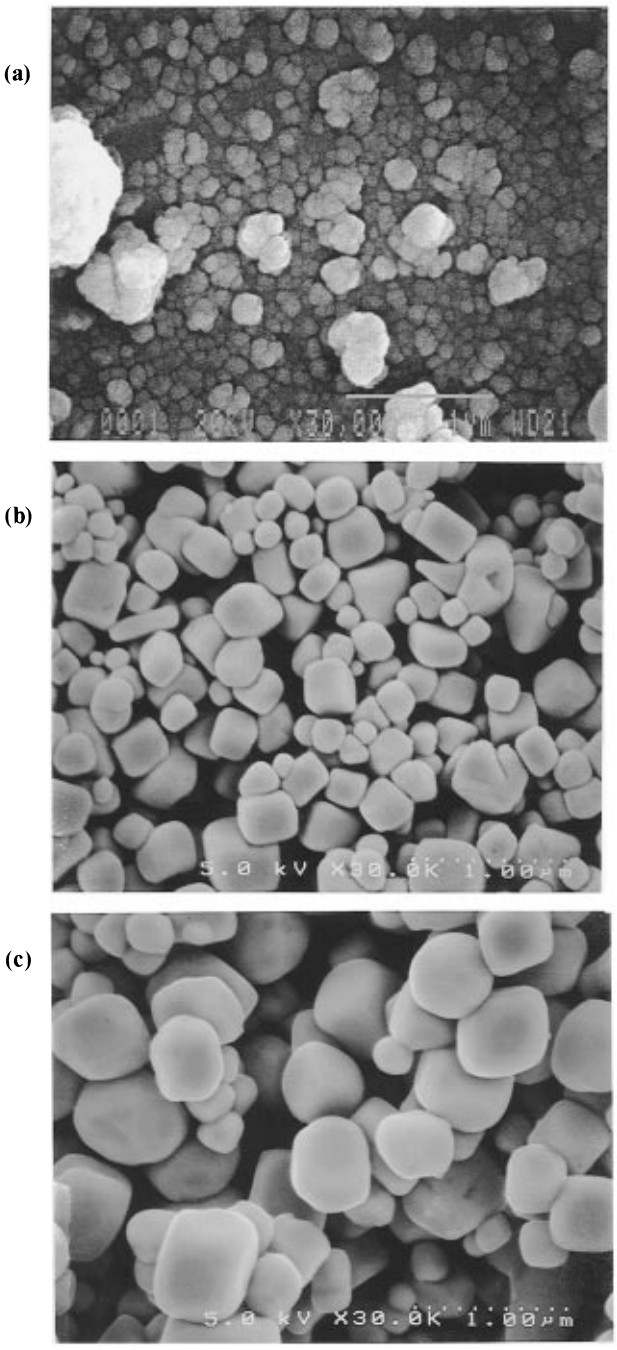

Figure 1. SEM micrographs of the $BaTiO_3$ powders: (a) A, (b) B, and (c) C.

quently discussed.[21] The formation of tetragonal $BaTiO_3$ was promoted by using barium chloride and hydrous titanium oxide with OH^- concentration of 1.0 M and a Ba/Ti ratio of 1.6.

In this work, the OH^- concentration was manipulated to form powders of varying particle sizes. At OH^- concentrations of 0.3 and 0.5 M, particles with average sizes of 0.09 and 0.3 μm were obtained after a week of synthesis at 240 °C. We refer to these as samples A and B. As the OH^- concentration was increased further to 4.0 M, we found that the average size decreases to 0.2 μm. For a starting concentration of 1.0 M NaOH, a continuous growth of the particles from 0.2 μm in the first week of synthesis to 0.5 μm after the eighth week

(21) Dutta, P. K.; Asiaie, R.; Akbar, S. A.; Zhu, W. *Chem. Mater.* **1994**, *6*, 1542.

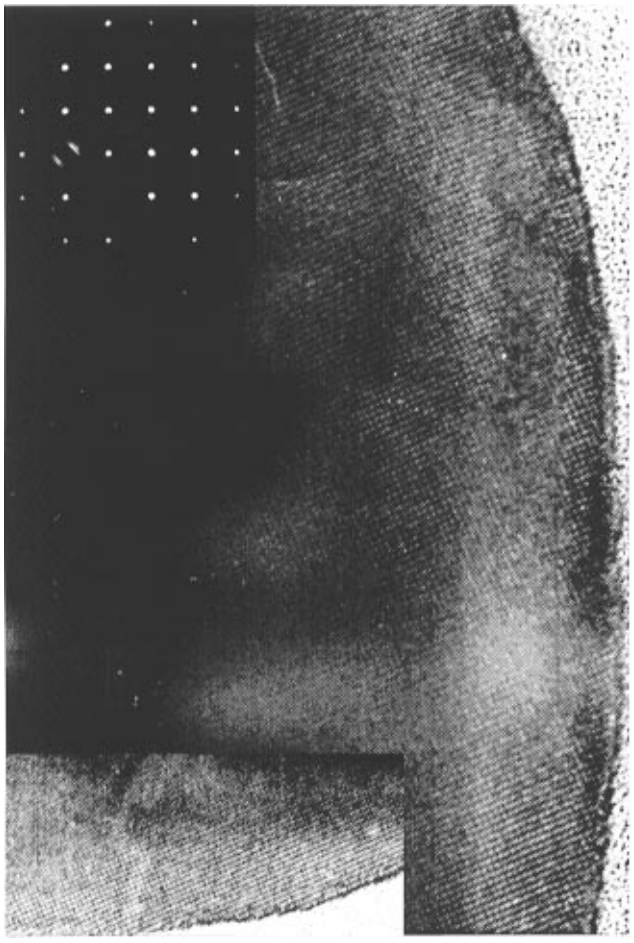

Figure 2. TEM micrographs of $BaTiO_3$ powder B (instrument magnification 500 000, enlarged by 10×).

was observed. Particle growth appeared to follow a ripening process, with larger particles appearing at longer times of synthesis. The growth rate could be manipulated by interrupting the synthesis and adding base to the reaction mixture during the synthesis. Thus, starting with an initial concentration of 0.5 M NaOH, and adding 0.003 mol of NaOH/10 mL of solution after a week of reaction and continuing the synthesis for another week resulted in particles with average size of 0.5 μm. We refer to this as sample C. The present study explores the structure of these three $BaTiO_3$ samples (A, B, C), and also contrasts these with a sample made by a classical hydrothermal synthesis at 95 °C.

The elemental composition, as determined by inductively coupled plasma spectroscopy were used to calculate Ba/Ti ratios of 0.53, 0.98, and 1.00 for samples A, B, and C, respectively. At the lowest pH for synthesis (sample A), considerable amounts of titanium oxide remain unreacted, with the $BaTiO_3$ accounting for 77 wt % of the material.

Structural Characteristics of the Hydrothermal Powders. Microscopy. The SEM micrographs of the three $BaTiO_3$ powders are shown in Figure 1. Powders B and C contain well-dispersed particles of reasonably uniform sizes of 0.3 and 0.5 μm, whereas sample A appears to be agglomerated with particle sizes of 0.09 μm. The powders were also examined using high-resolution transmission electron microscopy, and the micrographs are shown in Figure 2 for powders from sample B. There is no observable domain boundaries,

Table 1. Lattice and Lattice Strain Calculations of the $BaTiO_3$ Powders (A−C) As Determined by X-ray Diffraction

	sample		
	A	B	C
particle size by SEM (μm)	0.09	0.30	0.50
lattice parameter (Å)	$a = 3.9977 \pm 0.0021$ $c = 4.0272 \pm 0.0022$	3.9941 ± 0.0006 4.0362 ± 0.0008	3.9940 ± 0.0003 4.0357 ± 0.0005
c/a ratio	1.0078	1.0105	1.0104
lattice strain ($\times 10^3$)	0.763	0.408	0.216

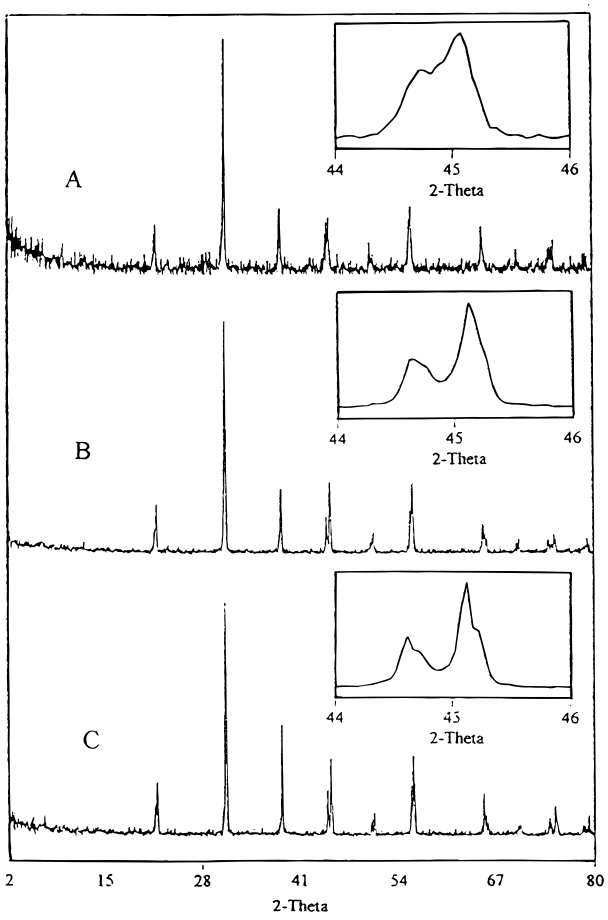

Figure 3. Powder X-ray diffraction patterns of the $BaTiO_3$ powders: A, B, and C.

and lattice fringes run continuously toward the interior of the particle. The image of the bottom part of the particle is shown in the left inset of the figure for clarity. For larger particles, as in sample C, the high-resolution image of the whole particle could not be obtained because the sample was too thick for the electron beam to transmit, and only areas very close to edge of the particles were observed. Since the lattice fringes at the opposite ends of the crystallite were similar, we propose that the crystallites have a single domain configuration. Convergent beam diffraction was also performed to confirm that the particles were single crystals. The upper right inset in Figure 2 shows the diffraction spot pattern with [001] incident beam direction obtained from a crystal of sample B. The diffraction patterns also suggest monodomain characteristics, since doubling of diffraction spots was not observed.[15b] Sample A consisted of both crystalline and amorphous particles. The particles were agglomerated with elementary particle sizes ranging from 50 to 100 nm. Crystalline particles could be readily distinguished from the amorphous ones, indicating incompleteness of the reaction.

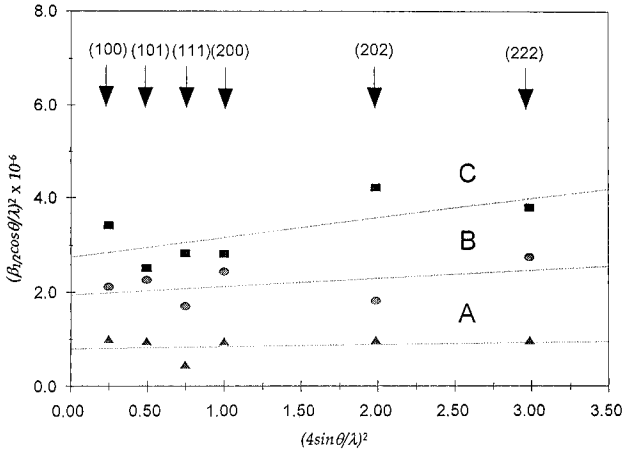

Figure 4. Hall−Williamson plots with Gaussian profile for the $BaTiO_3$ powders: A, B, and C.

X-ray Powder Diffraction. Figure 3 shows the X-ray powder diffraction patterns of samples A, B, and C and confirms that the crystalline material in these powders is only $BaTiO_3$. The unreacted material in sample A does not contribute to the diffraction pattern. This is reasonable, because it is unreacted titanium dioxide. The insets in Figure 3 show the reflections around 2θ of 45° [(200) + (020) and (002)]. The splitting of reflections in this region is a result of the distortion of the unit cell, characteristic of tetragonal $BaTiO_3$ and is enhanced from powders A−C. Lattice parameters (Table 1) calculated from the diffraction data indicate that the c/a ratios are 1.0078, 1.0105, and 1.0104 for samples A, B, and C, respectively.

The plots of $(\beta_{1/2} \cos \theta/\lambda)^2$ versus $(4 \sin \theta/\lambda)^2$ for each powder are shown in Figure 4. There is considerable scatter in the data, similar to a recent study on $PbTiO_3$.[22] From the slopes of these lines, the lattice strain was calculated and reported in Table 1. A decrease in strain from samples C through A is evident, though the overall magnitude of the strain is small (<0.001). The broadening of the diffraction primarily arises from the size of the samples, and a size of 58 nm was calculated for sample A. The unreacted Ti species in sample A should not influence these conclusions.

Vibrational Spectroscopy. *(a) Raman spectroscopy:* Figure 5a shows Raman spectra of powders A−C. The spectra have been displaced from each other to illustrate the similarities, in both peak frequencies and relative intensities. The amorphous material in sample A is not contributing to the spectrum. The spectra show a weak peak around 715 cm^{-1}, two strong and broad peaks around 515 and 260 cm^{-1}, and a sharp peak at 305 cm^{-1}. Factor group analysis for $BaTiO_3$ with cubic symmetry (space group $Pm3m = O_h^1$) predicts only

(22) Ishikawa, K.; Okada, N.; Takda, K.; Nomura, T.; Hagino, M. *Jpn. J. Appl. Phys.* **1994**, *33*, 3495

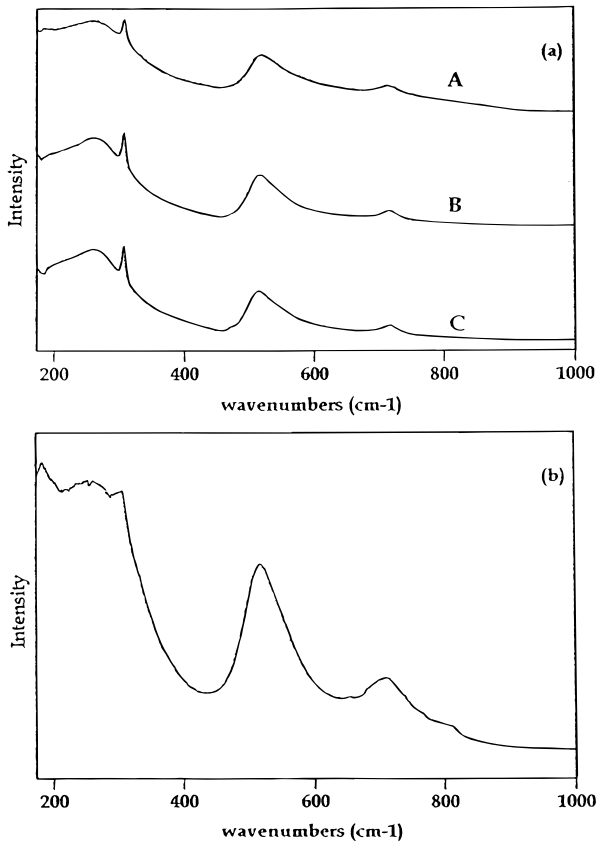

Figure 5. Raman spectra of the $BaTiO_3$ powders: (a) samples A, B, and C; (b) hydrothermally synthesized at 95 °C.

infrared bands:[23]

$$\Gamma_{optical} = 3F_{1u}\,(IR) + 1F_{2u}\,(inactive)$$

In the tetragonal symmetry (space group $P4mm = C_{4v}^1$),[23] 12 fundamental optical modes with the following irreducible representation are expected:

$$\Gamma_{optical} = 3A_1\,(IR\ \&\ R) + 4E\,(IR\ \&\ R) + B_1\,(R)$$

The cubic structure is formed with the Ti ion at the center of the unit cell, O ions centered on the six cube faces, and Ba ions on the cube corners. The structure may also be described as a system of TiO_6 octahedra joined at the corners with Ba ions placed in the interstitial positions between the octahedra. The tetragonal structure stems from development of a polar axis along the [100] direction. This polarization causes elongation of titanium and oxygen ions in opposite directions of the *c* axis. This causes the F modes to split into E and A_1 modes (F_{1u}) or E and B_1 modes (F_{2u}).

The Raman spectra of samples A−C are consistent with the spectrum of the tetragonal $BaTiO_3$ reported in the literature.[24] The bands around 515 and 260 cm^{-1} are assigned to the TO modes of A_1 symmetry, whereas the sharp peak at 305 cm^{-1} has been assigned to the

(23) Fateley, W. G.; Dollish, F. R.; McDevitt, N. T.; Bentley, F. F. *Infrared and Raman Selection Rules for Molecular and Lattice Vibrations*; Wiley: New York, 1972.

(24) (a) Javadpour, J.; Eror, N. G. *J. Am. Ceram. Soc.* **1988**, *71*, 206. (b) Rimai, L.; Parsons, J. L.; Hickmott, J. T.; Nakamura, T. *Phys. Rev.* **1968**, *168*, 623. (c) Didomenico, M.; Wemple, S. H.; Porto, S. P. S.; Bauman, R. P. *Phys. Rev.* **1968**, *174*, 522. (d) Chaves, A.; Katiyar, R. S.; Porto, S. P. S. *Phys. Rev.* **1974**, *B10*, 3522. (e) Perry, C. H.; Hall, D. B. *Phys. Rev. Lett.* **1965**, *15*, 700.

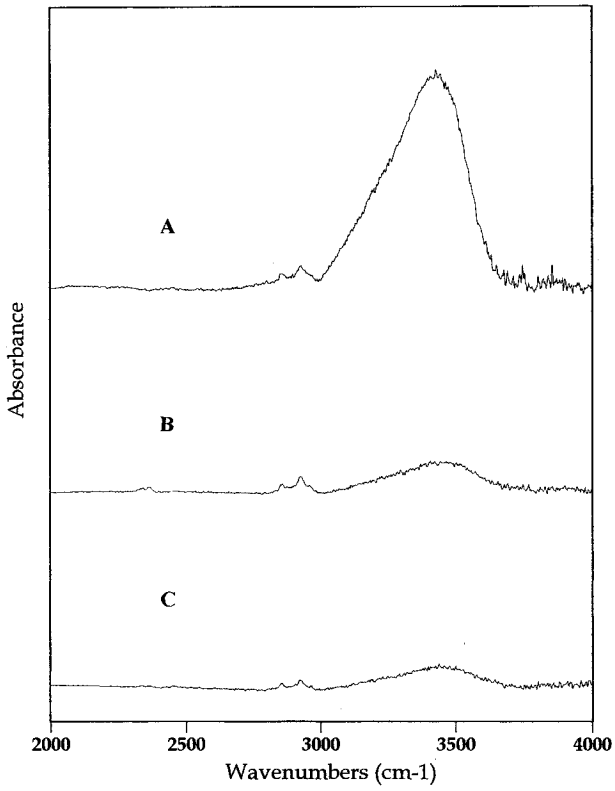

Figure 6. Infrared spectra of the OH stretching vibration region for the $BaTiO_3$ powders: A, B, and C.

B_1 mode. The weak band around 715 cm^{-1} has been associated with the highest frequency longitudinal optical mode (LO) of A_1 symmetry. The bands at 305 and 715 cm^{-1} disappeared upon heating above the Curie temperature. The presence of the two remaining bands above T_c, though the selection rules forbid Raman bands in the cubic form, has been noted before and assigned to second-order transitions. The Raman spectrum of the sample synthesized at 95 °C, which has been referred to as the metastable cubic form is shown in Figure 5b. Note that the sharpness of the 305 cm^{-1} is reduced, indicating partial tetragonality. The differences in absolute Raman intensities between the three powders (A−C) was attempted, but the precision of the method was too poor to make any judgements. This arose from the difficulty of focusing the laser reproducibly—use of an internal standard ($NaNO_3$) did not alleviate this problem for it was difficult to mix the two solids uniformly.

(b) Infrared spectroscopy: The two regions of the infrared spectrum of interest are the framework bands and the OH stretching region. Figure 6 shows infrared data of the OH stretching vibration around 3600 cm^{-1}. Since the samples for IR spectroscopy were prepared from powders heated to 110 °C under vacuum for 3 h, no interference from surface water is expected. Sample A contains considerably more hydroxyl groups than the other two samples. It is not possible to determine if the hydroxyl groups are arising from the $BaTiO_3$ or from the amorphous unreacted titanium dioxide, though it is very likely that it is the latter.

Figure 7a shows infrared spectra of the samples A−C in the framework region. Two broad bands around 560 and 431 cm^{-1} are observed. As Ruppin has pointed

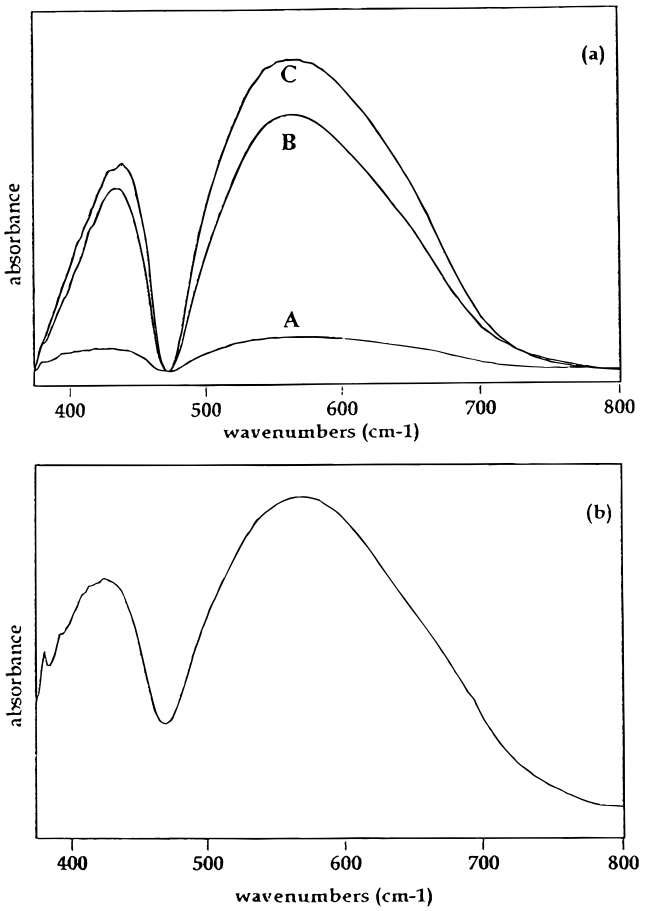

Figure 7. Infrared spectra of the $BaTiO_3$ framework region: (a) samples A, B, and C; (b) hydrothermally synthesized at 95 °C.

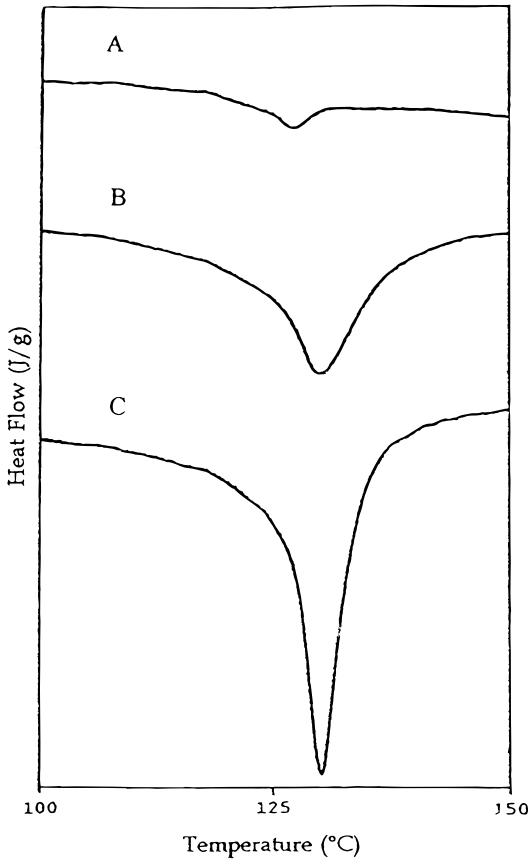

Figure 8. DSC traces for the $BaTiO_3$ powders: A, B, and C.

out,[25b] there are three types of optical phonon modes, transverse, longitudinal, and surface modes. The frequencies that we observe agree with the literature[25] and have been assigned to the surface modes. As the size of the particles become small compared to the wavelength of infrared radiation, there is uniform polarization of the particle and results in the surface or Frohlich modes. The profiles of the observed bands for all three particles A−C are similar— except that the half-width of the bands in sample A is about 25% greater, with contributions in the higher frequency part of the band. Two bands are also observed at slightly higher frequencies at 570 and 425 cm^{-1} for $BaTiO_3$ synthesized at 95 °C (Figure 7b).[25c]

The infrared spectra shown in Figure 7a for samples A−C were obtained from the same amounts of powder under identical conditions, and these intensities were reproducible to within 10% for different sample preparations. There is an increase in band intensities with increasing particle size. Correcting for the presence of unreacted TiO_2 (23 wt %) in sample A, the integrated band intensities for the 560 cm^{-1} increases in the order 1:9:13 for samples A−C, respectively.

Thermal Analysis of the Hydrothermal Powders. DSC curves around the Curie transition for powders A−C are presented in Figure 8. A transition between 125 and 130 °C is observed in each case, with enthalpies of transition (ΔH) 0.07, 0.50, and 0.85 J/g for particles A−C, respectively (making a numerical correction for the amorphous content in sample A). For completely tetragonal crystals, enthalpy of transition values of 0.73 and 0.84 J/g have been determined by DSC and specific heat measurements, respectively.[15b,c,26] The metastable cubic form synthesized at 95 °C did not exhibit any transition between ambient and 200 °C.

Hydroxyl content of the particles were obtained from the TGA curves (Figure 9), by estimating the weight loss between 200 and 600 °C. This loss corresponded to 0.6, 0.1, and 0.06 wt % decreases for the powders A−C, respectively. In terms of moles of OH groups lost from the sample A, we estimate about 8 mol %. In the other two samples, this fraction is less than 2.0 mol %. The weight loss above 800 °C due to CO_2 released from the decomposition of carbonate species was constant for all samples at 0.25 wt %. Even with precautionary measures, it was difficult to exclude CO_2 from leaking into the autoclave.

Discussion

Role of [OH^-] during Synthesis. Using $Ba(OH)_2$ as both the barium and base sources, it has been shown that the concentration of the base influences both the formation[10a] and kinetics of crystal growth of $BaTiO_3$.[10h] Hertl has reported that the rate of formation of $BaTiO_3$ becomes independent of $Ba(OH)_2$ at concentrations

(25) (a) Last, J. T. *Phys. Rev.* **1957**, *105*, 1740. (b) Ruppin, R. *Phys. Status Solifi B* **1974,** *64*, 701. (c) Diaz Guemes, M. I.; Gonzalez Carreno, T.; Serna, C. J. *Spectrochim. Acta* **1989**, *45A*, 589. (d) Busca, G.; Ramis, G.; Amores, J. M. G.; Escribano, V. S.; Piaggio, P. *J. Chem. Soc., Faraday Trans.* **1994**, *90*, 3181. (e) Ruppin, R. *J. Phys. C: Solid State Phys.* **1975**, *8*, 1969.

(26) Blattner, H.; Kanzig, W.; Merz, W. *Helv. Phys. Acta* **1949**, *22*, 35.

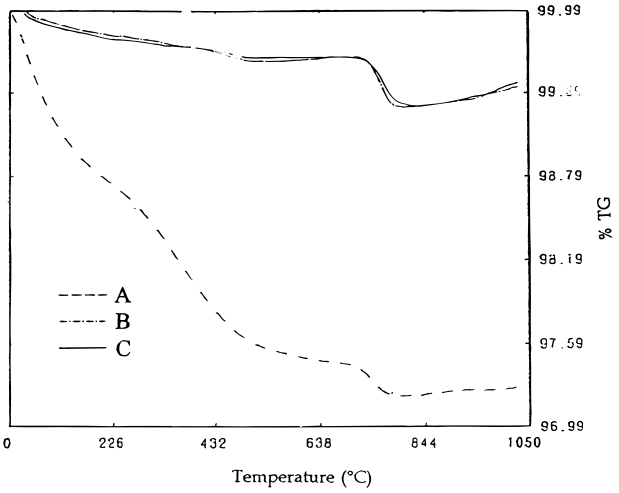

Figure 9. TGA of the $BaTiO_3$ powders: A, B, and C.

greater than 1 M of the base.[27] Hydrothermal formation of $BaTiO_3$ is stable under highly alkaline conditions,[10a,b] whereas neutral conditions destabilize these crystals.[10a,b,28]

In previous work, we proposed that $BaTiO_3$ particle growth occurred through a dissolution/recrystallization mechanism, indicating a ripening process.[21] The relevant chemical reaction is written as:

$$BaTiO_3\ (\text{small}) \rightarrow Ba^{2+} + Ti^{4+}\ \text{species} \rightarrow BaTiO_3\ (\text{large})$$

By varying the starting pH of the reactant composition, the OH^- concentration of 1 M was found to produce the largest crystallites but took 8 weeks. Since acidic conditions destabilize and basic conditions stabilize $BaTiO_3$, an optimum pH for rapid particle growth is expected. This can be accomplished by providing a buffer solution, which is difficult to do at high pH's. During synthesis the solution becomes acidic, which can be neutralized by addition of NaOH and results in accelerated particle growth.

To obtain smaller size crystallites, as in the case of sample A, the pH is not high enough to convert all the titanium species to $BaTiO_3$. It would be necessary to raise the pH to increase conversion, but that also increased the particle size. Since our goal was to examine the properties of $BaTiO_3$ as a function of particle size, we felt that the compromise of obtaining smaller crystals at the expense of not having complete conversion to $BaTiO_3$ was reasonable. Ideally, we would have liked to work with pure $BaTiO_3$, but, as we discuss below, the presence of the amorphous impurity does not influence our conclusions.

Comparison of the Microstructure of Samples A−C. *Particle Size*: The TEM micrographs show that the crystallites B and C are single crystals and consist of a single domain and sample A contains unreacted material. Size measurements by SEM microscopy indicate that the $BaTiO_3$ crystals for samples A−C are 0.09, 0.3, and 0.5 μm, respectively. Since the micrograph of sample A clearly showed the presence of agglomerates, particle size was also obtained from the X-ray peak-broadening analysis and found to be 58 nm. This is a better representation of the particle size.

Tetragonality. The Raman data suggest that all three $BaTiO_3$ powders possess tetragonal structure at the molecular level, and since the relative Raman peak intensities of all the peaks in these powders are similar, only tetragonal structure is present in these samples. If the crystals had a significant cubic component, then the Raman spectrum would resemble that of the hydrothermally synthesized $BaTiO_3$ at 95 °C (Figure 7b). This excludes the possibility that particles A−C contain tetragonal cores with surface cubic structure.[16a] Also, it is clear that the unreacted material in A is not causing any new bands in the spectrum. Unfortunately, we could not contrast the intensities between the samples to see if the magnitude of the polarizability in the crystals are changing as a function of size.

Infrared spectra of the powders show that Frohlich modes are being observed. The higher frequency contributions to the smallest particle A is consistent with the shift of surface modes to higher frequencies as the particle size decreases.[25b] Note that for surface modes to become effective in the Raman, particle sizes have to be considerably smaller, and this is not observed with samples A−C.[25e] Also of interest is the dramatic decrease of the overall intensity of the bands with particle size.

Defects: Sample A has more hydroxyl groups, as measured by both infrared and thermal analysis, and is probably arising from the unreacted material. However, with the larger particles B and C, OH groups are reduced and become essentially constant.

Strain: The strains in the three samples are distributed uniformly and are somewhat smaller (a factor of 2−5) as compared to that observed by Vivekanandan and Kutty.[15c] The lattice strain values showed a decreasing trend as a function of particle size but were overall small.

Goswami[17a] and Callaby[17b] proposed that the surface layer could diminish the dielectric constant, and its influence would increase with decreasing particle size. This would predict that the impurity could stabilize the metastable cubic form. However, from the Raman spectrum, it is seen that sample A has a tetragonal structure, and thereby we conclude that the presence of amorphous impurities does not necessarily imply transition to a cubic form. Thus, samples synthesized at 240 °C, regardless of the size, amorphousness, or presence of hydroxyl groups, remain in the tetragonal form.

Correlation of the Enthalpies of Transition with Structure. Previous reports have noted that ΔH decreases with particle size,[16] though it was unclear if the particles were tetragonal or metastable cubic. It is known that the enthalpy of transition (ΔH) is proportional to polarization (P):[29]

$$\Delta H = 2\pi P^2 T_c / C$$

where T_c is the transition temperature and C the Curie−Weiss constant. It can be seen that decrease of P will lead to a decrease in ΔH. From the ΔH, we

(27) Hertl, W. *J. Am. Ceram. Soc.* **1988**, *71*, 879.
(28) Osseo-Asare, K.; Arriagada, F. J.; Adair, J. H. *Ceram. Trans. Ceram. Powder Science II Am. Ceram. Soc.* **1988**, pp 47, 53.
(29) Burfoot, J. C. *Ferroelectrics: An Introduction to the Physical Principles*; 1967, p 64.

compute that the ratios of the polarization for samples A−C are 1.0:2.8:3.6.

Most explanations that have been proposed for the decrease of P relate to the change of the crystal structure from a tetragonal to cubic form. One prevalent explanation is that lattice defects and strains can force the structure to become cubic and P becomes equal to zero.[10d,15,30] The elimination of the strains by annealing results in tetragonal structure and increased ΔH. Studies of ZrO_2 also indicate that the metastable phases can be stabilized by defects and strains in the lattice.[31] Another explanation for the decrease in ΔH with particle size has been the surface tension.[32] The smaller the particle, higher internal hydrostatic pressure is thought to lower the Curie transition to below room temperature, thus leading to the cubic form. Increased surface energy of small particles in stabilizing the cubic form has also been proposed.[16]

However, in this study, particles A−C all appear to be tetragonal by spectroscopic criteria. The enthalpy change (ΔH) accompanying the Curie transition decreases from 0.85 J/g for sample C to 0.07 J/g for sample A. So then, we need to address why these samples, even though all tetragonal, show varying enthalpies of transition.

The enthalpy of transition has also been related with domain structure. A recent study of ground powders from sintered $BaTiO_3$ ceramics shows a decrease of ΔH as particle size is reduced.[33] The increased domain width and the subsequent decrease in domain concentration as the particles became smaller as well as decreased strain energy was thought to be reflected in the decrease in enthalpy. The formation of domains in $BaTiO_3$ ceramics has been attributed to large elastic strains during the Curie transition.[34] Since grains in a ceramic are clamped by their neighboring grains, a slight unit-cell dimension change during the transition leads to large elastic strains within the cells. Such large strains cause the entire state to be unstable. To relieve the strains, domains are formed in the ceramic grains. On the other hand, in unconstrained crystals, such as in this study, the crystals are able to change dimensions freely, so this elastic strain effect becomes minimal and should not be important. Since the powders A−C studied here are single domain structure with small lattice strain, the change in ΔH cannot be explained by lattice strains or domain concentrations.

The change in the local polarization near the surface is expected to occur over a distance comparable to the correlation length of polarization fluctuations. Ginzburg-Landau's mean field theory[35] has been successfully applied to study this effect on the magnetic properties of ferromagnetic particles.[36] Recently, this theory has been applied to ferroelectric thin films[37] and particles.[38] According to Landau's theory, the total free energy for a finite size and inhomogeneous ferroelectric can be expressed by a phenomenological equation using polarization (P) as an order parameter. The polarization can be expressed in terms of two parameters: correlation length (ξ) and extrapolation length (δ). The correlation length ξ is considered as a measure of the average distance over which the fluctuations of polarization are correlated. Larger ξ means a longer distance for the dipoles to interact with each other. This length is responsible for the temperature dependence of all physical quantities near the transition temperature. The extrapolation length δ describes the difference in coupling or ordering strength between the surface and the bulk. If the coupling strength of the bulk is larger than that of the surface, which is assumed to be the case in $BaTiO_3$, the surface will tend to be disordered as compared to the bulk. This surface disordering will force the bulk to disorder to a certain degree within a range defined by the correlation length ξ. Therefore, as particles become smaller, relatively more bulk, will be disordered. Eventually, the disordering will consume the entire bulk, and polar state will be destroyed. This is schematically illustrated in Figure 10. Wang et al.[38b] recently calculated the polarization as a function of particle size based on the mean-field theory and found that polarization decreases as the particle size gets smaller. Below a critical particle size of 44 nm for $BaTiO_3$, the polarization was predicted to drop down to zero and ferroelectricity would not be sustained. This mechanism appears to be most appropriate to explain the decrease in polarization observed with samples A−C. Recently, Schlag and co-workers[18] reported the DSC of samples along with their Raman spectra. Even though their samples were not completely tetragonal, as evidenced by the relative intensity of the 305 cm^{-1} band in the Raman, they also observed a decrease in ΔH as the particle size became smaller, and used Wang's model of disordering of dipoles to explain the decrease in P.

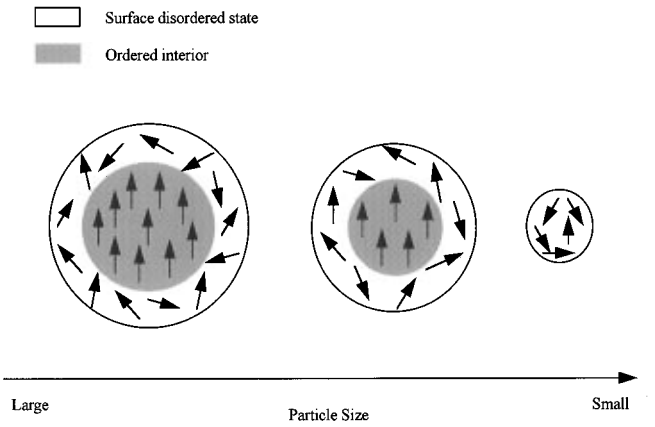

Figure 10. Schematic diagram to illustrate a particle from ordered to partially disordered and completely disordered as particle size decreases.

Another effect of the polarization is the presence of depolarizing fields.[39] The overall electrostatic energy

(30) (a) Kutty, T. R. N.; Padmini, P. *Mater. Res. Bull.* **1992**, *27*, 945. (b) Hennings, D.; Schreinemacher, S. *J. Eur. Ceram. Soc.* **1992**, *9*, 41.
(31) (a) Nishizawa, H.; Yamasaki, N.; Matsuoka, K. *J. Am. Ceram. Soc.* **1982**, *6*, 343. (b) Gravie, R. C. *J. Phys. Chem.* **1978**, *82*, 218.
(32) Uchino, K.; Sadanaga, E.; Hirose, T. *J. Am. Ceram. Soc.* **1989**, *72*, 1555.
(33) Hsiang, H.-I.; Yen, F.-S. *Jpn. J. Appl. Phys.* **1993**, *32*, 5029.
(34) (a) Merz, W. J. *Phys. Rev.* **1954**, *95*, 690. (b) Arlt, G. *Ferroelectrics* **1987**, *76*, 451.
(35) Ginzburg, V. L.; Landau, L. D. *JETP 20* **1950**, 1064.
(36) Kumar, P. *Phys. Rev.* **1974**, *B10*, 2928.
(37) (a) Binder, K. *Ferroelectrics* **1981**, *35*, 99. (b) Tilley, D. R.; Zeks, B. *Solid State Commun.* **1984**, *49*, 823.
(38) (a) Cottam, M. G.; Tilley, D. R.; Zeks, B. *J. Phys. C: Solid State Phys.* **1984**, *17*, 1793. (b) Wang, Y. G.; Zhong, W. L.; Zhang, P. L. *Solid State Commun.* **1994**, *90*, 329.
(39) Batra, I. P.; Wurfel, P.; Silverman, B. D. *Phys. Rev.* **1973**, *8*, 3257.

can be minimized by neutralization of the field by the formation of domains. When the crystal becomes smaller, the rapid increase of domain wall energy makes the domain configuration unfavorable, thereby promoting single-domain structure in smaller crystals, as we observe in samples A−C. Whether this size-dependent intracrystalline field is responsible for the increase in intensity of the infrared transitions observed in samples A−C is at present unclear.

The $BaTiO_3$ powders examined in this study remain tetragonal down to a size of 90 nm (58 nm by XRD), i.e., the TiO_6 octahedra are distorted. However, as particles become smaller, there is a disordering of the bulk dipoles, resulting gradually in transition from a polar to a nonpolar state. This is coupled with an expected decrease in *c*/*a* ratio as observed from sample C to A. There is also a modest increase in strain as the particles become smaller in size. The origin of this strain could arise from the increased disordering of the dipoles, though this is somewhat speculative. On the basis of the data for sample A, we can also state that the completely nonpolar form should appear below a crystallite size of 90 nm (58 nm by XRD). The predictions of the theory by Wang and co-workers are that this transition should occur at 44 nm.

Conclusions

The major conclusions of this study are as follows:

Tetragonally distorted $BaTiO_3$ crystals are grown at 240 °C under hydrothermal conditions.

Hydroxyl defects, strain, or the presence of amorphous impurity do not induce the tetragonal crystals to assume a metastable cubic form.

Enthalpy of transition decreases due to disordering of the dipoles, resulting in a particle-size-dependent transition from polar to nonpolar form.

The intensity of the infrared bands decreases with decreasing crystallite size.

Acknowledgment. We would like to acknowledge funding from the National Science Foundation (NSF DMR-9202565). We acknowledge helpful discussions with Profs. P. Gallagher and J. Lannutti, Mr. B. Gaskins, and Dr. Z. Zhong.

CM950327C